Insolation Cycles as a Major Control of Equatorial Indian Ocean Primary Production

Luc Beaufort,* Yves Lancelot, Pierre Camberlin, Olivia Cayre, Edith Vincent, Franck Bassinot, Laurent Labeyrie

Analysis of a continuous sedimentary record taken in the Maldives indicates that strong primary production fluctuations (70 to 390 grams of carbon per square meter per year) have occurred in the equatorial Indian Ocean during the past 910,000 years. The record of primary production is coherent and in phase with the February equatorial insolation, whereas it shows diverse phase behavior with $\delta^{18}O$, depending on the orbital frequency (eccentricity, obliquity, or precession) examined. These observations imply a direct control of productivity in the equatorial oceanic system by insolation. In the equatorial Indian Ocean, productivity is driven by the wind intensity of westerlies, which is related to the Southern Oscillation; therefore, it is suggested that a precession forcing on the Southern Oscillation is responsible for the observed paleoproductivity dynamics.

Reconstructing past variations of primary production during Pleistocene climatic cycles is an important requirement for estimating the effects of the ocean's biological pump on the atmospheric CO_2 concentration through time (*1*). Because primary production in many oceanic areas is closely related to wind stress, paleoproductivity reconstructions should also provide information about climate dynamics. Here we analyzed variations in primary production through time in the equatorial Indian Ocean, as recorded in sediments from a giant piston core (MD900963) taken in the Maldives area (Fig. 1). The equatorial Indian Ocean is particularly interesting because winds are strongest during spring and fall (*2*), in contrast with the rest of the Indian Ocean where winds reach their maximum during summer (southwest monsoon) and winter (northeast monsoon). These intermonsoon winds, called the Indian Ocean equatorial westerlies (IEW) (*3*), result from the zonal (Walker) circulation along the equator (*4*). The IEW are positively correlated to the Southern Oscillation (SO) index (*3*), which is a measure of the intensity of the Walker circulation (*5*).

Although the IEW are climatically important, their intermillenium variability is not yet known because most of the previous paleoclimatic records in the Indian Ocean were established in areas dominated by monsoon winds, such as the Somalian margin (*6*), the Arabian Sea (*7, 8*), and the Bay of Bengal (*9*). In contrast, core MD900963 was recovered beneath the narrow equatorial track (7°N to 7°S) along which the IEW prevail, providing a continuous record for investigating the dynamics of primary production associated with the IEW for the last 910,000 years (ky).

The 54-m-long piston core MD900963, retrieved during the SEYMAMA expedition of the research vessel *Marion Dufresne* east of the Maldives (5°03.30′N, 73°53.60′E; Fig. 1) at a water depth of 2446 m, consists primarily of carbonate ooze. Oxygen isotope measurements on planktonic foraminifera provide a detailed stratigraphic framework. To develop an astronomical age model for core MD900963, Bassinot *et al.* (*10*) tuned (adjusted in frequency) this $\delta^{18}O$ record (*11*) on the Imbrie and Imbrie ice volume model (*12*). The resulting chronology is in good accordance with the ice volume model used as a tuning target, but the ages appear to be consistently slightly younger (900 years) than the ages obtained by correlating the $\delta^{18}O$ record to the SPECMAP stack (*13*). This small shift mainly results from slight, initial phase differences in the Milankovitch bands between the SPECMAP record (21 June) and the ice volume model (mid July) (*13*). With the 10-cm sampling interval the record has a time resolution of about 2000 years.

Here we analyze the coccolithophore assemblages. Coccolithophores, a major phytoplanktonic group, are reliable recorders of oceanic productivity (*14*). At low latitudes, the coccolithophore communities of the lower photic zone (~60 to ~180 m) are dominated by *Florisphaera profunda*. Most of the other species live in the upper part of the photic zone (0 to ~60 m) (*15*). This vertical zonation has been used successfully for paleoproductivity studies (*14, 16*), where the abundance of *F. profunda* in fossil assemblages was used to monitor the depth

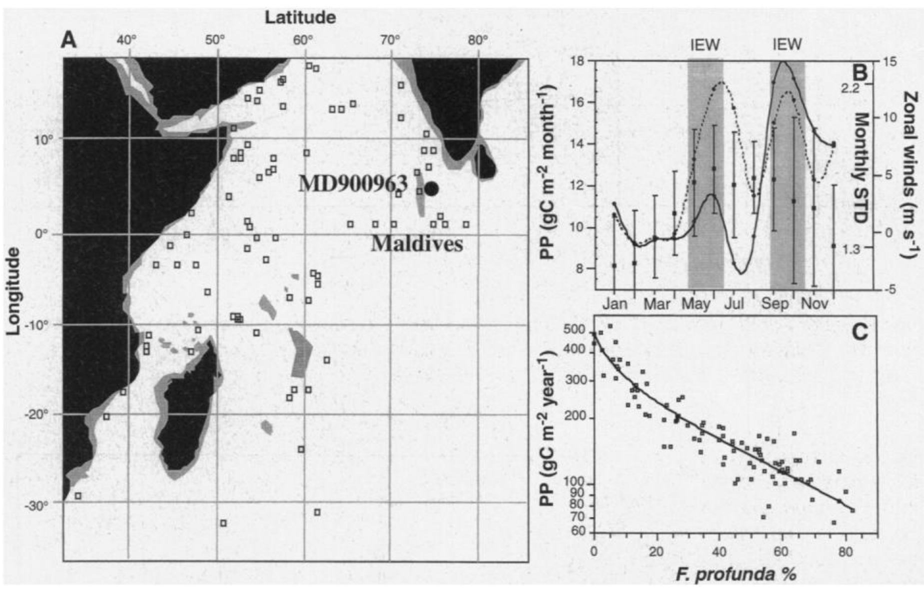

Fig. 1. (**A**) Location of core MD900963 and core tops (squares) used for calibration (10 core tops located out of the mapped area are not shown). (**B**) Comparison of the monthly PP estimates (solid line) (*16*), based on satellite information obtained from the open ocean east of the Maldives (0° to 5°N and 74° to 75°E), with monthly variability of zonal wind at 5°N, 73°E from the COADS Atlas (*34*). Squares represent averaged monthly wind speed (1947 to 1992) with interannual variability (2σ error bars), and the dashed line corresponds to the intramonth standard deviation averaged from 1947 to 1992. (**C**) Calibration of the percentage of *F. profunda* to modern PP. The yearly PP estimates (*16*) are based on satellite information. The solid line corresponds to the best regression equation {$y = 617 - [279 \times \log(x + 3)]$, $r = 0.94$}. The mean absolute value of the residuals is ± 26 gC m^{-2} $year^{-1}$.

L. Beaufort, Y. Lancelot, O. Cayre, E. Vincent, Laboratoire de Géologie du Quaternaire du CNRS, CEREGE, Boite Postale 80, 13545 Aix-en-Provence Cedex 4, France.
P. Camberlin, Centre de Recherches de Climatologie, Université de Bourgogne, Boite Postale 138, 21004 Dijon Cedex, France.
F. Bassinot and L. Labeyrie, Centre des Faibles Radioactivités, CNRS-CEA, Avenue de la Terrasse, 91198 Gif-sur-Yvette Cedex, France.

*To whom correspondence should be addressed. E-mail: beaufort@cerege.fr

of the nutricline. The relative abundance of *F. profunda* increases when the upper photic zone is impoverished in nutrients and the nutricline is deep. Conversely, *F. profunda* decreases in relative abundance when wind stress induces a rise of the nutricline and an increase of primary production in the upper photic zone.

To calibrate this marker to primary production we counted ~400 coccoliths to estimate the relative abundance of *F. profunda* (Fp) in 96 superficial sediment samples taken from a large variety of environments in the Indian Ocean (Fig. 1A). We found that Fp is highly correlated with primary production (hereafter referred to as PP) estimated from satellite information (*17*) (Fig. 1C). Using the least squares method we tested different types of equations to determine the best fit for the distribution of Fp versus PP. The best correlation ($r = 0.94$) was with the equation

$$\mathrm{PP} = 617 - [279 \times \log(\mathrm{Fp} + 3)] \quad (1)$$

In core MD900963, there are large variations of Fp ranging from 5 to 85%. On the basis of Eq. 1, these variations indicate PP variations ranging from 70 to 390 grams of carbon (gC) $\mathrm{m^{-2}\ year^{-1}}$ (Fig. 2). The average PP in the core record is 180 gC $\mathrm{m^{-2}\ year^{-1}}$, which is close to the modern value of 163 gC $\mathrm{m^{-2}\ year^{-1}}$ at this location (*17*). These variations of PP span almost the entire range of values of the modern Indian Ocean. Paleoproductivity estimated from independent indicators for the last 160 ky in core MD900963 [organic carbon abundance, concentration of alkenones (*18*), and absolute abundance of coccoliths (*19*)] is in very good agreement with the productivity deduced from the abundance of *F. profunda*. Planktonic foraminifera also provide independent paleoproductivity estimates in core MD900963. Foraminifera species were counted in 136 samples corresponding to the last 270 ky, and the assemblages were analyzed by principal component analysis (PCA) (*20*). Assemblages of North Indian Ocean core tops stored in the world data base (*21*) were introduced as additional samples in the PCA. The resulting first factorial coordinates were calibrated with the PP data from satellite information (*17*). The linear regression calculated between the PCA coordinates and PP ($r = 0.73$) was used as a transfer function to estimate PP in core MD900963. The PP estimations derived from foraminifera are similar to those obtained from *F. profunda* (Fig. 3). The similarity of these independent estimations validates the PP record in terms of both relative variations and absolute values of PP.

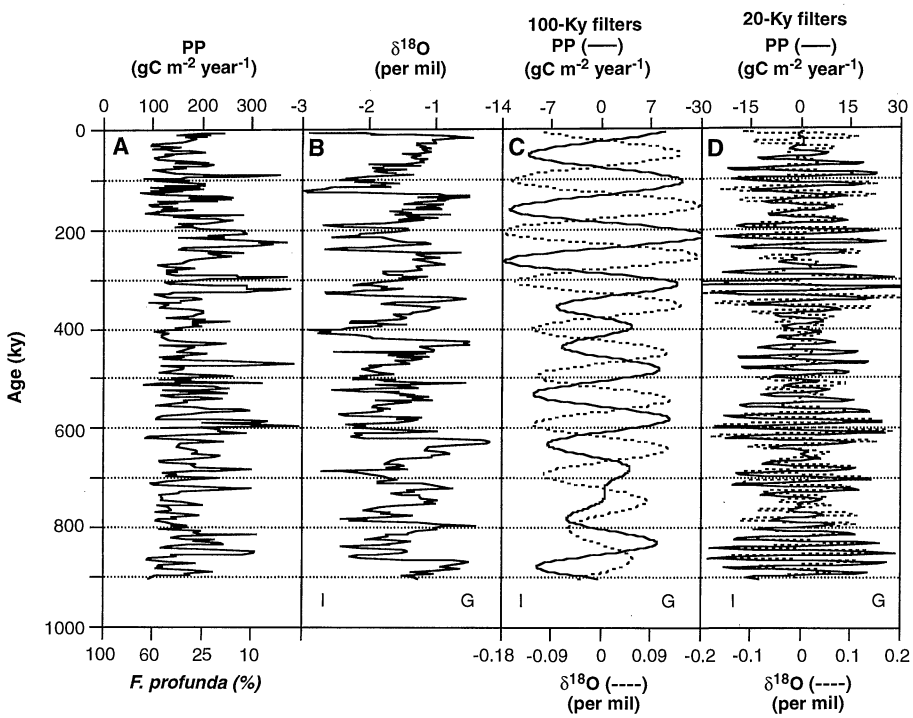

Fig. 2. Record of PP (**A**) and of the $\delta^{18}O$ measured from the planktonic foraminifera *Globigerinoides ruber* (**B**). Gaussian band-pass filters applied to PP (solid line) and to $\delta^{18}O$ (dotted line) centered at 100 ky (**C**) and 20 ky (**D**). G and I refer to glacial and interglacial.

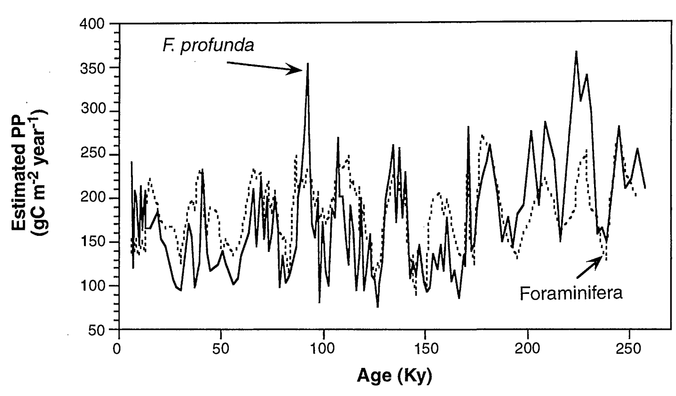

Fig. 3. Comparison of PP estimates obtained from *F. profunda* (solid line) and planktonic foraminifera (dashed line) counts for the last 270 ky in core MD900963.

We computed time series analyses of the *F. profunda* productivity record using maximum entropy, Blackman-Tukey, and multi-Taper (*22*) methods. All three revealed significant periods of 350, 120, 88, 42, 23.8, 22.5, and 19 ky, which correspond closely to Earth's orbital periods of eccentricity (404, 123.8, and 94.8 ky), obliquity (41.1 ky), and precession (23.7, 22.4, and 19.0 ky) (*23*) (Fig. 4A). The significance of these frequencies was tested by performing a cross-spectral analysis between pp and a stack of the normalized orbital forcing functions (eccentricity, tilt, and precession) (*13*). The two signals are highly coherent in the eccentricity band (122 ky) and at the three precession periods (23.8, 22.32, and 19.2 ky) (Fig. 4B).

Cross-spectral analysis reveals that productivity and ice volume ($\delta^{18}O$) are anticorrelated in the eccentricity band (Fig. 4C), whereas they are almost in phase in the precession band. The filtered data show clearly this phase behavior (Fig. 2, C and D). Furthermore, phase analysis indicates that productivity maxima lead ice volume maxima (high values of the $\delta^{18}O$ record) by ~2800 years in the precession band. The PP record is highly coherent and in phase with variations of the late winter equatorial insolation, and it is also in phase with the eccentricity.

Classically, the spectral signature of most paleoceanographic proxies during the Pleistocene exhibits the 100-, 41-, and 23- to 19-ky periods in decreasing order of magnitude. This is attributed to a major influence of continental ice sheets in the northern latitudes on internal dynamics after the 100-ky cycle and to the effect of these ice sheets on global climate (*24*). As for some other tropical paleoclimatic records (*14*, *25*), the Maldives PP record is dominated by precession cycles. However, the PP record is also characterized by significant phase variations with respect to $\delta^{18}O$, from one orbital frequency to the other, which has not been observed in these other paleoclimatic proxies. Both the dominance of the 23- to 19-ky periods in the PP variability and its phase behavior relative to the 100-ky period strongly suggest that the main climatic factor driving the PP variations is directly controlled by the insolation. The 100-ky component of the PP record may result in part from the smaller influence of ice sheets at the equator. It may also reflect a nonlinear response of PP to low-latitude insolation forcing inducing a transfer of power from the envelope of precession (23 to 19 ky), which is amplitude-modulated by changes in Earth's eccentricity (*24*). The PP record has a lower asymptote around 70 gC m^{-2} $year^{-1}$, which may correspond to a minimum level of PP in that area. As a consequence, the response of PP is truncated below a given insolation threshold. Such a truncated response produces energy at the frequencies corresponding to the modulation of precession. The presence of a 400-ky cycle in the PP record, which is indicated both in the frequency domain (Fig. 4) and in the time domain by the decrease in the amplitude of the 100-ky cycle around 400,000 and 800,000 years B.P. (Fig. 2C), supports that interpretation because that feature does not appear in $\delta^{18}O$ records.

At the location of core MD900963, wind atlases indicate that the westerlies blow significantly from May through November (Fig. 1B). Intramonth variability increases strongly during the IEW season (May to June and October and November). This variability results from a succession of strong bursts capable of generating greater mixing of the surface water in the photic zone and may explain why modern PP reaches its highest levels during the IEW seasons, particularly in the fall (Fig. 1B). The zonal winds in October and November accounted for 41% of the mean annual variability between 1946 and 1992 and are significantly correlated to major climatic anomalies, and in particular to the SO ($r = +0.44$ between the SO index and October-November zonal winds at 5°N, 73°W, becoming $r = +0.67$ nearer the equator). In contrast, the smaller Maldives summer wind variability (24% for July and August) is not significantly correlated to any meteorological factor (the best correlation is with the intensity of the Indian monsoon with $r = -0.24$). The interannual variability of PP should follow that of the IEW and the SO. In any case, the 23- to 19-ky cycles observed in the wind-driven PP fluctuations cannot correspond to past monsoon dynamics because the summer monsoon paleorecords have negative phases ranging from −100° to −150° with the summer solstice (*8*), whereas the PP record has a positive phase of 118°.

If the IEW interannual variability is linked to the SO, then a correlation should exist between the Maldives and the eastern equatorial Pacific PP records, because the interannual variability of upwelling in the eastern equatorial Pacific is controlled by the intensity of the trade winds, which are in turn linked to the SO. The Maldives PP-insolation phase is similar to that of the eastern equatorial Pacific PP records, which lead precession by about 102° to 126° and $\delta^{18}O$ by about 24° to 48° (*26*). Those synchronous records in the precession band are indicative of an influence of the SO on both regions on a millennium time scale. In the eccentricity band, however, the Pacific and Maldives records are opposite in phase. In the eastern equatorial Pacific, the oceanographic variability is driven by variation of the strength of local trade winds in the precession bands, and by global climatic factors in the eccentricity band (*27*). Therefore, comparisons of SO records in the Maldives and eastern equatorial Pacific are significant only in the precession frequency band.

The Maldives PP record belongs to a group of paleoceanographic markers that respond to precession in advance relative to global ice volume variations. This group includes proxies from the equatorial Pacific and southern oceans, whereas the Milankovitch theory implies a lead of the Northern Hemisphere (*28*). Our study shows that equatorial climatic and hydrographic conditions may have varied independently from global ice volume and, therefore, could explain the original response of equatorial conditions to insolation forcing. If insolation acts directly on the SO, it would be possible to determine during which season insolation drives the highest SO response because this phenomenon occurs on time scales much shorter than a thousand years. The 118° lead of PP over the 21 June insolation indicates that PP maxima are in phase with solar radiation maxima in February [centered on 26 February or on 6 February when the chronologies from Bassinot *et al.* (*10*) and SPECMAP (*13*) are used]. The importance of the past February insolation may tentatively be compared with observations showing that boreal winter (and particularly February) is a key season in SO mod-

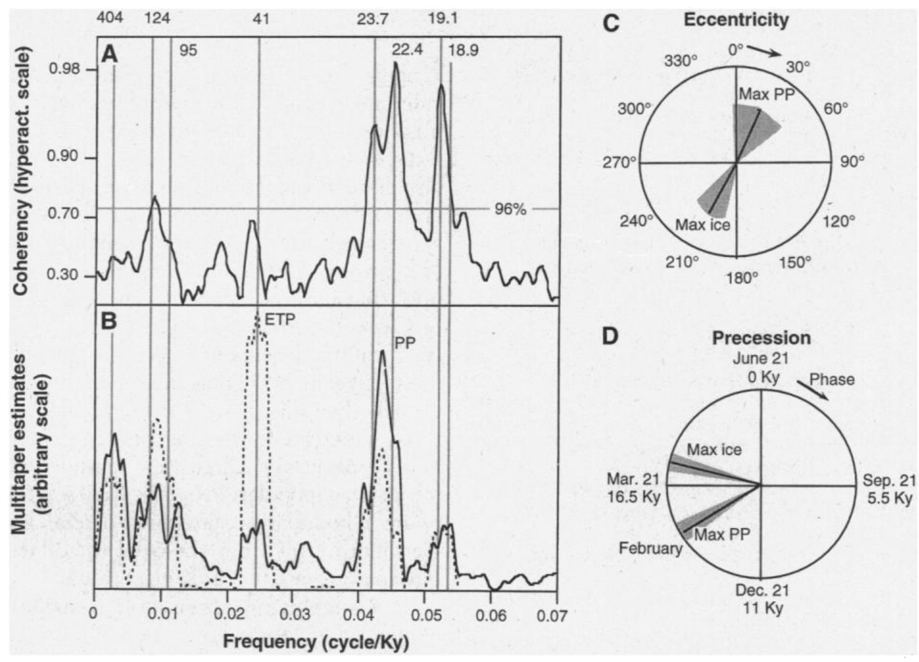

Fig. 4. Time series analysis. (**A**) Coherency (Cross-Blackman-Tukey) between PP and a normalized, summed time series of Earth's eccentricity, obliquity (tilt), and precessional parameters (ETP). The horizontal line denotes the 96% confidence level. (**B**) Multi-Taper analysis (*22*) of PP (solid line) and ETP (dashed line). Vertical gray lines in (A) and (B) indicate orbital frequencies [period in thousand years on top of (A)]. (**C**) Phase diagram of PP and $\delta^{18}O$ for eccentricity (dashed areas correspond to band pass). (**D**) Phase diagram of PP and $\delta^{18}O$ for precession (dashed areas indicate band pass). The origin is chosen for a summer solstice insolation maximum. Other seasonal maxima are also reported on the diagram scale. PP maxima are in phase with insolation maxima in February.

ulation: Yanusari found that February characterizes the beginning of the El Niño cycle (29), and that in February (i) the amplitude and variability of the principal interannual atmospheric mode associated with the SO are highest (30) and (ii) the tropical convection that may lead to the onset of El Niño–Southern Oscillation (31) is strongest (31, 32).

In conclusion, we have shown that an equatorial climatic mechanism produces strong variations of PP in the Indian Ocean. This mechanism is directly related to insolation and independent from global ice volume variations. It may be linked to past dynamics of the SO. If this mechanism acted over most of the equatorial ocean, the related PP variations could have produced a significant effect on global climates.

REFERENCES AND NOTES

1. W. S. Broecker, *Prog. Oceanogr.* **11**, 151 (1982); R. S. Keir and W. H. Berger, *J. Geophys. Res.* **88**, 6027 (1983); N. J. Shackleton, M. A. Hall, J. Line, C. Shuxi, *Nature* **306**, 319 (1983).
2. R. A. Knox, in *Monsoons,* J. S. Fein and P. L. Stephens, Eds. (Wiley, New York, 1987), pp. 365–398.
3. S. Hastenrath, A. Nicklis, L. Greischar, *J. Geophys. Res.* **98**, 20219 (1993).
4. H. Flohn, *Bonn. Meteorol. Abh.* **15**, 1 (1971).
5. J. Bjerkness, *Mon. Weather Rev.* **97**, 163 (1969).
6. J.-P. Caulet, M. Vénec-Peyré, C. Vergnaud-Grazzini, C. Nigrini, in *Upwelling Systems: Evolution Since the Early Miocene,* C. P. Summerhayes, W. L. Prell, K. C. Emeis, Eds. (Geological Society Special Publication, London, 1992), pp. 379–389.
7. W. L. Prell and W. B. Curry, *Oceanol. Acta* **4**, 91 (1981); F. Sirock *et al.*, *Nature* **364**, 322 (1993); K. C. Emeis, D. M. Anderson, H. Doose, D. Kroon, D. Schulz-Bull, *Quat. Res.* **43**, 355 (1995).
8. S. C. Clemens and W. L. Prell, *Paleoceanography* **5**, 109 (1990).
9. J. C. Duplessy, *Nature* **295**, 494 (1982); M. R. Fontugne and J.-C. Duplessy, *Palaeogeogr. Palaeoclimatol. Palaeoecol.* **56**, 69 (1986); A. Sarkar *et al.*, *Nature* **343**, 549 (1990).
10. F. C. Bassinot *et al.*, *Earth Planet. Sci. Lett.* **126**, 91 (1994).
11. The formula for $\delta^{18}O$ is as follows, where the standard is the standard NBS reference 19:

$$\delta^{18}O = \frac{(\delta^{18}O/\delta^{16}O)_{\text{sample}} - (\delta^{18}O/\delta^{16}O)_{\text{standard}}}{(\delta^{18}O/\delta^{18}O)_{\text{standard}}} \times 1000$$

12. J. Imbrie and J. Z. Imbrie, *Science* **207**, 943 (1980).
13. J. Imbrie *et al.*, in *Milankovitch and Climate,* A. Berger, J. Imbrie, J. Hays, G. Kukla, B. Saltzman, Eds. (NATO ASI Series C, Reidel, Dordrecht, Netherlands, 1984), vol. 1, pp. 269–306.
14. B. Molfino and A. McIntyre, *Science* **249**, 766 (1990).
15. H. Okada and S. Honjo, *Deep Sea Res.* **20**, 355 (1973).
16. A. McIntyre and B. Molfino, *Science* **274**, 1867 (1996).
17. D. Antoine, J. M. André, A. Morel, *Global Biogeochem. Cycles* **10**, 57 (1996).
18. F. Rostek *et al.*, in *Global Precipitations and Climate Changes,* M. Desbois and F. Désalamand, Eds. (NATO ASI Series I, Reidel, Dordrecht, Netherlands, 1994), pp. 27–51.
19. L. Beaufort, *Quat. Int.* **31**, 13 (1996).
20. O. Cayre, L. Beaufort, E. Vincent, *Quat. Sci. Rev.* in press.
21. W. L. Prell, "The Stability of Low-Latitude Sea-Surface Temperatures: An Evaluation of the CLIMAP Reconstructions with Emphasis on the Positive SST Anomalies" (Report TR. 025, U.S. Department of Energy, Washington, DC, 1985).
22. D. J. Thomson, *Proc. IEEE* **70**, 1055 (1982).
23. A. Berger and M.-F. Loutre, *Quat. Sci. Rev.* **10**, 297 (1991).
24. J. Imbrie *et al.*, *Paleoceanography* **8**, 699 (1993).
25. E. M. Pokras and A. C. Mix, *Nature* **326**, 486 (1987).
26. These precession phases are from the following sources: (i) the $\Delta\delta^{13}C$ series from core V19-30, which leads $\delta^{18}O$ by 1.8 ky and the orbital parameters by 117° (33) [equivalent to 102° using Bassinot *et al.* (10) chronology] {J. Imbrie *et al.* (28) give a slightly different phase of 141° [equivalent to 126° using the Bassinot *et al.* (10) chronology]}; and (ii) the Corg MAR record from core V19-28, which leads $\delta^{18}O$ by 28° (equivalent to an ETP lead of 108° in our chronology) [M. Lyle, *Nature* **335**, 529 (1988)].
27. M. W. Lyle *et al.*, *Nature* **355**, 812 (1992).
28. J. Imbrie *et al.*, *Paleoceanography* **7**, 701 (1992).
29. T. Yasunari, *Bull. Am. Meteorol. Soc.* **72**, 1331 (1991).
30. K.-M. Lau *et al.*, *J. Atmos. Sci.* **51**, 1169 (1994).
31. K.-M. Lau and P.-H. Chan, *ibid.* **45**, 506 (1988).
32. M. L. Salby and H. H. Hendon, *ibid.* **51**, 2207 (1994).
33. N. J. Shackleton and N. G. Pisias, in *The Carbon Cycle and Atmospheric CO_2: Natural Variations Archean to Present,* E. T. Sundquist and W. S. Broecker, Eds, (American Geophysical Union Geophysical Monograph 32, American Geophysical Union, Washington, DC, 1985), pp. 303–317.
34. S. D. Woodruff, R. J. Slutz, R. L. Jenne, P. M. Steurer, *Bull. Am. Meteorol. Soc.* **68**, 1239 (1987).

35. We thank C. P. Summerhayes, W. H. Berger, and two anonymous reviewers who helped improve the manuscript. Supported by funding from Institut National des Sciences de l'Univers/CNRS under Programme National d'Etude de la Dynamique du Climat and Dynamique de la Terre et Evolution des Climats programs. The PP data are available on the World Wide Web at www.cerege.fr. This is contribution 97038 of Laboratoire de Géologie du Quaternaire–CNRS.

25 March 1997; accepted 16 October 1997

Connectivity and Management of Caribbean Coral Reefs

Callum M. Roberts

Surface current patterns were used to map dispersal routes of pelagic larvae from 18 coral reef sites in the Caribbean. The sites varied, both as sources and recipients of larvae, by an order of magnitude. It is likely that sites supplied copiously from "upstream" reef areas will be more resilient to recruitment overfishing, less susceptible to species loss, and less reliant on local management than places with little upstream reef. The mapping of connectivity patterns will enable the identification of beneficial management partnerships among nations and the design of networks of interdependent reserves.

Populations of marine organisms are typically much more open than terrestrial populations. The great majority of species have a dispersive pelagic larval stage, and many also disperse as eggs. Currents transport eggs and larvae, sometimes for long distances, generating interconnections among areas (1). Strong connectivity among areas implies that local populations may depend on processes occurring elsewhere. Consequently, local management initiatives may be ineffective in providing local benefits (although they may benefit other areas), and thus an increase in the scale of management may be necessary. Large-scale connectivity means that populations will often straddle political boundaries, sometimes several, and identifying which nations need to collaborate may seem to be a daunting task.

If a simplifying assumption is made—namely, that larvae are dispersed passively by currents—then surface current patterns should reveal routes of larval transport and patterns of connectivity (Fig. 1A). Potential connections among areas of the Caribbean (2) were mapped for dispersal periods of 1 and 2 months, which encompasses larval duration for the majority of reef species (3). For 18 locations with coral reefs, "transport envelopes" were mapped from which larvae spawned elsewhere could potentially arrive and to which larvae spawned locally could potentially be transported (Fig. 1, B and C). Measures of reef area within these envelopes reveal that from place to place in the Caribbean, there is an order of magnitude variation in both upstream and downstream reef area (Fig. 2).

Upstream reef area provides an indication of potential larval supply. At the low end of the scale, Barbados is almost entirely dependent on local larval production to replenish populations. By contrast, Andros Island, in the Bahamas, and reefs in the middle Florida Keys can draw larvae from very large catchments. Places with large upstream reef areas should be more resilient to recruitment overfishing (that is, fishing at intensities high enough that populations are limited by insufficient reproduction), because depletion of local populations may be offset by inputs of offspring spawned elsewhere. For example, Jamaica's reefs have been intensively fished since the end of the last century (4). Populations of many

Environment Department, University of York, York YO1 5DD, UK. E-mail: cr10@york.ac.uk